



# Nonlinear finite element simulation of unbonded prestressed concrete beams

Leandro S. Moreira<sup>b</sup>, João Batista M. Sousa Jr.<sup>a,\*</sup>, Evandro Parente Jr.<sup>a</sup>

<sup>a</sup> Laboratório de Mecânica Computacional e Visualização, Universidade Federal do Ceará, Brazil

<sup>b</sup> Universidade Federal do Ceará, Campus Crateús, Brazil



## ARTICLE INFO

### Keywords:

Prestressed concrete  
Unbonded tendons  
Nonlinear analysis  
Prestressing tendon

## ABSTRACT

Prestressed concrete with internal unbonded tendons has been recognized as an excellent structural option for beams and slabs and is employed worldwide. Numerical solutions for the analysis of such structures are still an active field of research. This work presents a finite element model for the physical and geometrical nonlinear analysis of prestressed concrete beams with unbonded internal tendons, under short-term loading. The reinforced concrete beam is modeled by Euler-Bernoulli nonlinear plane frame elements and a total Lagrangian approach. The prestressing tendon is modeled by a single polygonal element embedded in a specified subset of the frame elements. Due to lack of strain compatibility between the concrete and the tendon at a given cross-section, the cable strain is computed from the displacements of all associated frame elements. Geometric and material nonlinearities are considered for both the reinforced concrete beam and the prestressing tendons. The internal force vector and corresponding tangent stiffness matrix of each element under large displacements are derived consistently, and novel expressions for the tangent stiffness operator which ensure the convergence rates of the Newton-Raphson scheme are developed. The accuracy of the formulation is assessed by comparison with experimental tests, with very good results.

## 1. Introduction and literature overview

Prestressed concrete structures are mainly divided into two groups, according to the application of the prestressing forces to the concrete element. Pretensioning considers that the steel is tensioned before the concrete is cast, therefore requiring bond between the elements for the proper force transfer. Post-tensioning, on the other hand, implies that the tendon or cable applies stresses upon the concrete element already during the prestressing operation. In this case the bond between prestressing steel and concrete depends on the constructive solution adopted.

Unbonded prestressed concrete structures are a very efficient load-carrying system, especially with the use of greased low-cost tendons protected by plastic sheathing. These elements have been used extensively in North America for over 50 years [1] and have become popular in the construction of medium rise buildings in Brazil in the last decades.

The numerical simulation of these structures is a challenging task, as one must necessarily cope with the first stages of application of tensioning, the immediate loss of prestress, the behavior under external loads and, in case of a long-term analysis, the loss of prestress due to phenomena such as shrinkage, creep and tendon relaxation.

Numerical analysis of unbonded prestressed concrete beams tends

to be more complex than that of the bonded case, since in the former there is no strain compatibility between the concrete and the tendon at a given cross-section. Thus, the cable strain depends on the displacements of the tendon as a whole.

The crucial issue, therefore, is the consideration of the slipping tendon. The most employed strategy has its roots on the load balancing concept, which was originally introduced by Lin and Burns [2] and afterwards extended by Aalami [3,4]. According to this approach, the tendon acts as an external force applied to the concrete beam.

The FE simulation of mechanical behavior of prestressed concrete beams with unbonded tendons is still the subject of various research works. In the following some of the most recent ones, more closely related to the present work, are briefly described.

Barbieri et al. [5] developed a hybrid FE model for bonded and unbonded prestressed concrete frames, where the active and passive reinforcements are modeled as layers within the cross section. The bonded tendon contributes to the overall stiffness, but the unbonded tendon is considered as an equivalent force which does not contribute to the stiffness coefficients.

D'Allasta and Zona [6] developed a FE model for externally prestressed composite beams with deformable connection. Later the same research group presented a formulation for nonlinear analysis of beams prestressed with external slipping tendons [7], as well as analytical and

\* Corresponding author.

E-mail address: [joabatistasousajr@hotmail.com](mailto:joabatistasousajr@hotmail.com) (J.B.M. Sousa).

simplified procedures for prestressed beams [8–10]. Their FE model takes into account the influence of the tendon change of position in the tangent stiffness matrix in the context of a high order displacement-based FE formulation.

Lou and Xiang [11,12] developed a numerical procedure to investigate second-order effects on externally prestressed concrete beams. Later, Lou et al. [13,14] included the effect of long-term behavior on the nonlinear analysis of prestressed concrete girders within a similar nonlinear FE formulation. The same authors have also applied their numerical formulation for beams prestressed with FRP tendons [15,16], for prestressed concrete columns [17] and externally prestressed steel-concrete composite beams [18].

Vu and coworkers [19] developed a nonlinear FE model for the structural response of post-tensioned beams, based on a so-called macro finite element which is characterized by its homogeneous average inertia. Kim and Lee [20] developed a flexural analytical model focused on the behaviour of continuous unbonded post-tensioned members.

The present work focuses on the analysis of prestressed concrete beams with unbonded internal tendons, under short-term loading. The reinforced concrete beam is modeled by nonlinear plane frame elements based on the Euler-Bernoulli-Navier beam theory and the total Lagrangian approach. Each unbonded tendon is modeled by a single polygonal element embedded in the correspondent the frame element. Geometric and material nonlinearities are considered for both the reinforced concrete beam and the prestressing tendons. The internal force vector and tangent stiffness matrix of each element under large displacements are derived in a variationally consistent way, providing optimal rates of convergence to the nonlinear analysis procedure. Special attention is given to the development of consistent and robust numerical approaches for the two stages of short-term loaded prestressed concrete beams: tendon stressing and further load application. The accuracy of the formulation is assessed by comparison with experimental results.

## 2. Frame element

The proposed model employs an Euler-Bernoulli displacement-based frame element for the simulation of the reinforced concrete member. The hypotheses of plane sections, with large displacements and moderate rotations, widely used on analysis of reinforced concrete frames, are considered in the context of a Total Lagrangian description. The displacement field can be written as:

$$u(X,Y) = u_0(X) - Y v'_0(X) \quad v(X,Y) = v_0(X) \quad (1)$$

where  $u$  and  $v$  are the axial and transverse displacements and the subscript 0 refers to displacements at the beam reference axis. The element geometry and coordinate system are shown in Fig. 1. The analytical model considers the membrane  $\varepsilon_0$  and curvature  $\kappa$  terms, with the geometric nonlinearity taken into account in the membrane strain as follows:

$$\varepsilon = u'_0 + \frac{1}{2} v_0'^2 - Y v'' = \varepsilon_0 - Y \kappa \quad (2)$$

The membrane strain and the curvature can be interpreted as generalized strains and written in vector form as:

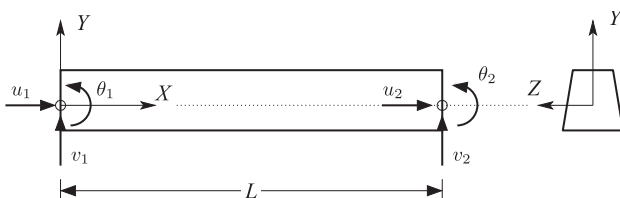


Fig. 1. Frame element geometry and degrees of freedom.

$$\varepsilon = \begin{bmatrix} \varepsilon_0 \\ \kappa \end{bmatrix} = \begin{bmatrix} u'_0 \\ v_0'' \end{bmatrix} + \frac{1}{2} \begin{bmatrix} v_0'^2 \\ 0 \end{bmatrix} \quad (3)$$

where the first and second vector represents the linear ( $\varepsilon_L$ ) and non-linear ( $\varepsilon_{NL}$ ) generalized strains.

The axial stresses ( $\sigma$ ) can be computed from the axial strains ( $\varepsilon$ ) using the constitutive models discussed in Section 4, while the normal force ( $N$ ) and bending moment ( $M$ ), henceforth called generalized stresses, are computed from the integration of stresses in the cross-section:

$$\sigma = \begin{bmatrix} N \\ M \end{bmatrix} = \begin{bmatrix} \int_A \sigma \, dA \\ - \int_A Y \sigma \, dA \end{bmatrix} \quad (4)$$

The element degrees of freedom (DOFs) are depicted in Fig. 1. The usual beam minimum continuity requirements imply the use of a  $C^0$  linear and  $C^1$  cubic hermitian interpolation functions for the axial and transverse displacements, respectively. Let  $L_i(x)$  be the two axial linear interpolants and  $H_i(x)$  be the four transverse interpolant functions. The introduction of these functions allows the representation of the generalized strains from the nodal displacements via the strain-displacement matrices

$$\varepsilon = \mathbf{B} \mathbf{u}_e = (\mathbf{B}_L + \frac{1}{2} \mathbf{B}_{NL}) \mathbf{u}_e \quad (5)$$

where  $\mathbf{B}_L$  and  $\mathbf{B}_{NL}$  are respectively the linear and nonlinear strain-displacement matrices and  $\mathbf{u}_e$  is the nodal displacement vector of the element. Matrix  $\mathbf{B}_L$  contains derivatives of the interpolation functions  $L_i$  and  $H_i$  and is the same for linear beam elements, as may be seen in any textbook on linear finite elements. For this reason the focus will be on the nonlinear strain-displacement term. The source for nonlinearity is the term  $v_0'^2$ .

From the displacement interpolation, the term  $v_0'$ , equal to the cross-section rotation ( $\theta$ ) can be written as:

$$v_0' = \theta = [0 \quad H_1' \quad H_2' \quad 0 \quad H_3' \quad H_4'] \mathbf{u}_e = \mathbf{G} \mathbf{u}_e \quad (6)$$

Thus, the nonlinear part of the membrane strain is given by:

$$\varepsilon_{NL} = \frac{1}{2} v_0'^2 = \frac{1}{2} \mathbf{u}_e^T \mathbf{G}^T \mathbf{G} \mathbf{u}_e \quad (7)$$

This expression contains polynomial terms  $n \times x$  up to quartic, while  $\varepsilon_L$  is constant along the element. The unbalanced higher order terms can lead to membrane locking due to inability to represent membrane strains associated with inextensional bending [21]. In order to avoid membrane locking, a higher-order interpolation for the axial displacements was adopted in [7], increasing the number of degrees of freedom and the element complexity. A simpler approach is adopted here, whereby the average strain [21] is used instead of the original expression: Thus:

$$\varepsilon_{NL} = \frac{1}{2} \frac{1}{L} \int_0^L v_0'^2 \, dX = \frac{1}{2} \mathbf{u}_e^T \mathbf{A} \mathbf{u}_e \quad (8)$$

where

$$\mathbf{A} = \frac{1}{L} \int_0^L \mathbf{G}^T \mathbf{G} \, dX \quad (9)$$

Matrix  $\mathbf{A}$  is symmetric, constant and can be evaluated analytically, producing a nonlinear strain vector

$$\varepsilon_{NL} = \frac{1}{2} \begin{bmatrix} \mathbf{u}_e^T \mathbf{A} \\ \mathbf{0} \end{bmatrix} \mathbf{u}_e = \mathbf{B}_{NL} \mathbf{u}_e \quad (10)$$

where the implemented form of  $\mathbf{B}_{NL}$  is shown. Incrementally, with a view to virtual work application, it can be shown that the following holds:

$$\delta \varepsilon = (\mathbf{B}_L + \mathbf{B}_{NL}) \delta \mathbf{u}_e = \bar{\mathbf{B}} \delta \mathbf{u}_e \quad (11)$$

The element internal force vector ( $\mathbf{g}_e$ ) can be obtained from the

internal virtual work:

$$\delta U_e = \int_0^L \delta \varepsilon^T \sigma dX = \delta \mathbf{u}_e^T \int_0^L \bar{\mathbf{B}}^T \sigma dX = \delta \mathbf{u}_e^T \mathbf{g}_e \quad (12)$$

The tangent stiffness matrix required by the nonlinear analysis procedure based on Newton-Rapshon iterations is symmetric, and can be obtained by the differentiation of  $\mathbf{g}_e$  w.r.t. the nodal displacements:

$$\mathbf{K}_{T_e} = \frac{\partial \mathbf{g}_e}{\partial \mathbf{u}_e} = \mathbf{K}_{E_e} + \mathbf{K}_{G_e} \quad (13)$$

The material stiffness matrix is given by

$$\mathbf{K}_{E_e} = \int_0^L \bar{\mathbf{B}}^T \mathbf{C}_T \bar{\mathbf{B}} dX \quad (14)$$

where the tangent section constitutive matrix is obtained from the differentiation of the generalized stresses with respect to the generalized strains

$$\mathbf{C}_T = \begin{bmatrix} \frac{\partial N}{\partial \varepsilon_0} & \frac{\partial N}{\partial \kappa} \\ \frac{\partial M}{\partial \varepsilon_0} & \frac{\partial M}{\partial \kappa} \end{bmatrix} \quad (15)$$

The geometric stiffness matrix is given by

$$\mathbf{K}_{G_e} = \int_0^L N A dX \quad (16)$$

Due to the material nonlinearity of the concrete and rebars, the cross-section generalized stresses ( $\sigma$ ) and tangent constitutive matrix ( $\mathbf{C}_T$ ) should be evaluated using appropriate procedures, as the fiber method for path-dependent materials or special integration techniques for nonlinear elastic materials [22–24]. Integration on the element length is carried out using Gauss or Lobatto rules. The fiber method and Gauss integration are used in the examples of this work.

### 3. Unbonded tendon element

In unbonded prestressed beams, as depicted in Fig. 2, there is no strain or even displacement compatibility between the sliding tendon and the embedding concrete. Thus, the tendon and the concrete have the same displacement only at the anchorage points. As a consequence, the tendon strain cannot be evaluated by means of a cross-section analysis, requiring the consideration of the whole structure deformation [25,26].

Similar to [13], the proposed model considers the curved unbonded prestressing tendon as an assemblage of straight segments. However, in [13] the tendon is considered as an external force, while in the present work the tendon is considered as a finite element, contributing not only to the internal force vector, but also to the tangent stiffness matrix.

Considering that the tendon slides without friction inside the plastic sheathing, the strain along the tendon is uniform and equal to the average strain of the surrounding concrete. So, the tendon stress is considered constant along the cable length. The endpoints of each straight segment are linked to the RC element degrees of freedom, as shown in Fig. 3.

It is important to note that the coordinates of each tendon segment do not correspond to the same material point, which slides relative to the concrete section, but rather to the coordinates of the plastic sheathing, which is considered perfectly bonded to the surrounding concrete. These coordinates are then employed to evaluate the variation of the tendon length and subsequently its strain. From the tendon

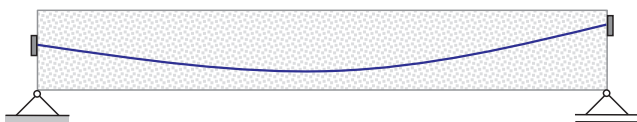


Fig. 2. Unbonded prestressed beam.

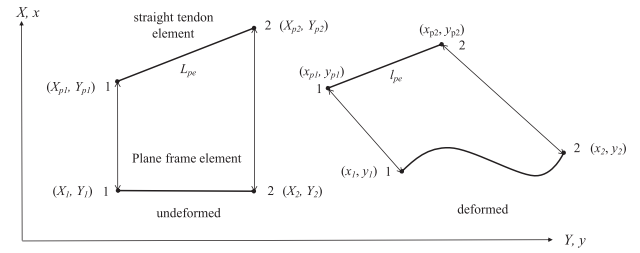


Fig. 3. Frame element and tendon segment before/after deformation.

strain, it is possible to evaluate the contribution of the tendon to the total virtual work of the prestressed beam and obtain the internal force vector and the consistent tangent stiffness of the tendon element, as shown in the following.

The displacements of the straight tendon segment are obtained from the displacement of the embedding frame element substituting its end coordinates in Eq. (1):

$$\begin{aligned} u_{p1} &= u_1 - Y_1 \theta_1 \\ v_{p1} &= v_1 \\ u_{p2} &= u_2 - Y_2 \theta_2 \\ v_{p2} &= v_2 \end{aligned} \quad (17)$$

where  $u_{p1}, u_{p2}$  are the axial displacements and  $v_{p1}, v_{p2}$  are the vertical displacements of the straight segment end points. This expression can be written in matrix form as

$$\begin{bmatrix} u_{p1} \\ v_{p1} \\ u_{p2} \\ v_{p2} \end{bmatrix} = \begin{bmatrix} 1 & 0 & -Y_1 & & & \\ 0 & 1 & 0 & & & \\ & & & 1 & 0 & -Y_2 \\ & & & 0 & 1 & 0 \end{bmatrix} \begin{bmatrix} u_1 \\ v_1 \\ \theta_1 \\ u_2 \\ v_2 \\ \theta_2 \end{bmatrix} \quad (18)$$

or in compact form

$$\mathbf{u}_{pe} = \mathbf{T}_e \mathbf{u}_e \quad (19)$$

where  $\mathbf{u}_{pe}$  is the end displacement vector of the tendon segment,  $\mathbf{u}_e$  is the displacement vector of the embedding frame element and  $\mathbf{T}_e$  is a transformation matrix which depends only on the undeformed coordinates of the segment end points. On the other hand, the displacements of the embedding element can be related to the global displacement vector ( $\mathbf{u}$ ) of the complete finite element model by

$$\mathbf{u}_e = \mathbf{L}_e \mathbf{u} \quad (20)$$

where  $\mathbf{L}_e$  is a Boolean localization matrix relating the degrees of freedom of a tendon segment  $e$  with the global degrees of freedom. Thus, the segment displacements can be directly related to the global displacements:

$$\mathbf{u}_{pe} = \mathbf{T}_e \mathbf{L}_e \mathbf{u} \quad (21)$$

As the strain is assumed constant along the tendon length, the internal virtual work associated with its deformation is given by:

$$\delta U_p = \int_{L_p} \int_{A_p} \delta \varepsilon_p \sigma_p dA dS = \delta \varepsilon_p F_p L_p \quad (22)$$

where  $F_p = A_p \sigma_p$  is the tendon force and  $L_p$  is the initial (i.e. undeformed) tendon length. The tendon strain is given by the sum of a constant initial strain  $\varepsilon_{p0}$  and the incremental displacement-dependent strain ( $\Delta \varepsilon_p$ ):

$$\varepsilon_p = \varepsilon_{p0} + \Delta \varepsilon_p \quad (23)$$

The initial strain  $\varepsilon_{p0}$ , which does not have a physical meaning in the case of post-tensioning, corresponds to a reference strain value whose interpretation is provided later in this paper. The incremental strain is defined conveniently as the engineering strain [21] leading to the following definition of total strain:

$$\varepsilon_p = \varepsilon_{p0} + \frac{\ell_p - L_p}{L_p} = \varepsilon_{p0} + \frac{\sum_{e=1}^{n_p} (\ell_{pe} - L_{pe})}{\sum_{e=1}^{n_p} L_{pe}} \quad (24)$$

where  $L_{pe}$  and  $\ell_{pe}$  are the initial and deformed segment lengths, as depicted in Fig. 3, and  $n_p$  is the number of tendon segments.

The strain variation used in the evaluation of the virtual work can be obtained from the previous equation as

$$\delta\varepsilon_p = \frac{\delta\ell_p}{L_p} \quad (25)$$

After some manipulation, the variation of a segment length can be written as:

$$\delta\ell_{pe} = \frac{(x_{pj} - x_{pi})}{\ell_{pe}} (\delta x_{pj} - \delta x_{pi}) + \frac{(y_{pj} - y_{pi})}{\ell_{pe}} (\delta y_{pj} - \delta y_{pi}) \quad (26)$$

or

$$\delta\ell_{pe} = \cos\beta (\delta u_{uj} - \delta u_{ui}) + \sin\beta (\delta v_{uj} - \delta v_{ui}) \quad (27)$$

where  $\beta$  is the angle of the deformed segment with the horizontal axis. This equation can be conveniently cast in matrix form as

$$\delta\ell_{pe} = \begin{bmatrix} -\cos\beta & -\sin\beta & \cos\beta & \sin\beta \end{bmatrix} \begin{bmatrix} \delta u_{pi} \\ \delta v_{pi} \\ \delta u_{pj} \\ \delta v_{pj} \end{bmatrix} = \mathbf{r}_e^T \delta \mathbf{u}_{pe} \quad (28)$$

where  $\delta \mathbf{u}_{pe}$  are the virtual displacements of the tendon segment. Summing up the contributions for all the elements which form the tendon yields the variation of the current length:

$$\delta\ell_p = \sum_{e=1}^{n_p} \delta\ell_{pe} = \sum_{e=1}^{n_p} \mathbf{r}_e^T \mathbf{T}_e \delta \mathbf{u}_e \quad (29)$$

Therefore, the internal virtual work of the prestressing tendon is given by

$$\delta U_p = \delta\ell_p F_p = \sum_{e=1}^{n_p} \delta\ell_{pe} F_p = \sum_{e=1}^{n_p} \mathbf{r}_e^T \mathbf{T}_e \delta \mathbf{u}_e F_p \quad (30)$$

This equation can be written in a compact form as

$$\delta U_p = \sum_{e=1}^{n_p} \mathbf{g}_{pe}^T \delta \mathbf{u}_e \quad (31)$$

where the internal force vector of the each tendon segment is

$$\mathbf{g}_{pe} = \mathbf{T}_e^T \mathbf{r}_e F_p \quad (32)$$

or

$$\mathbf{g}_{pe} = \mathbf{w}_e F_p = \begin{bmatrix} -\cos\beta \\ -\sin\beta \\ Y_i \cos\beta \\ \cos\beta \\ \sin\beta \\ -Y_j \cos\beta \end{bmatrix} F_p \quad (33)$$

where  $\mathbf{w}_e = \mathbf{T}_e^T \mathbf{r}_e$ . It is important to note that, in Eq. (32), vector  $\mathbf{r}_e$  depends only on the segment displacements, while the tendon force  $F_p$  depends on the global displacement vector  $\mathbf{u}$ .

From Eq. (20),  $\delta \mathbf{u}_e = \mathbf{L}_e \delta \mathbf{u}$ . Thus, the tendon contribution to the global internal force is given by

$$\mathbf{g}_p = \sum_{e=1}^{n_p} \mathbf{L}_e^T \mathbf{g}_{pe} \quad (34)$$

In the actual computer implementation, the global internal force vector of the prestressing tendon can be obtained using the classical finite element assembly operator:

$$\mathbf{g}_p = \mathbf{A} \begin{pmatrix} \mathbf{g}_{pe} \end{pmatrix}_{e=1}^{n_p} \quad (35)$$

The tendon global tangent stiffness  $\mathbf{K}_{Tp}$  is obtained straightforwardly from the differentiation of the global internal force vector with respect to the nodal displacements:

$$\mathbf{K}_{Tp} = \frac{\partial \mathbf{g}_p}{\partial \mathbf{u}} = \sum_{e=1}^{n_p} \mathbf{L}_e^T \frac{\partial \mathbf{g}_{pe}}{\partial \mathbf{u}} \quad (36)$$

Differentiating Eq. (32) with respect to the nodal displacements, one gets

$$\frac{\partial \mathbf{g}_{pe}}{\partial \mathbf{u}} = \mathbf{T}_e^T \frac{\partial \mathbf{r}_e}{\partial \mathbf{u}} F_p + \mathbf{T}_e^T \mathbf{r}_e \frac{\partial F_p}{\partial \mathbf{u}} \quad (37)$$

Therefore, the tangent stiffness matrix of the tendon is given by

$$\mathbf{K}_{Tp} = \sum_{e=1}^{n_p} \left( \mathbf{L}_e^T \mathbf{T}_e^T \frac{\partial \mathbf{r}_e}{\partial \mathbf{u}} F_p + \mathbf{L}_e^T \mathbf{T}_e^T \mathbf{r}_e \frac{\partial F_p}{\partial \mathbf{u}} \right) \quad (38)$$

The second term of the r.h.s. can be identified as the material stiffness matrix. The tendon force derivative with respect to the nodal displacements is given by

$$\frac{\partial F_p}{\partial \mathbf{u}} = A_p \frac{\partial \sigma_p}{\partial \varepsilon_p} \frac{\partial \varepsilon_p}{\partial \mathbf{u}} = \frac{A_p E_{pt}}{L_p} \sum_{a=1}^{n_p} \mathbf{r}_a^T \mathbf{T}_a \mathbf{L}_a \quad (39)$$

where the index  $a$  was introduced because the tendon force  $F_p$  depends on the displacements of the whole tendon and not only on those of segment  $e$  in Eq. (38). Therefore, the material stiffness matrix of the tendon can be written as

$$\mathbf{K}_{Ep} = \left( \frac{E_{pt} A_p}{L_p} \right) \mathbf{w} \mathbf{w}^T \quad (40)$$

where

$$\mathbf{w} = \sum_{e=1}^{n_p} \mathbf{L}_e^T \mathbf{w}_e = \mathbf{A} \begin{pmatrix} \mathbf{w}_e \end{pmatrix}_{e=1}^{n_p} \quad (41)$$

Thus,  $\mathbf{K}_{Ep}$  is a symmetric and dense matrix whose dimension depends on the beam discretization, since it connects the degrees of freedom of the nodes of all embedding elements.

The first term of the r.h.s. of Eq. (37) corresponds to the geometric stiffness matrix of the tendon segment. The derivative of the vector  $\mathbf{r}_e$  with respect to the global displacement vector is given by

$$\frac{\partial \mathbf{r}_e}{\partial \mathbf{u}} = \frac{\partial \mathbf{r}_e}{\partial \mathbf{u}_e} \frac{\partial \mathbf{u}_e}{\partial \mathbf{u}} = \frac{\partial \mathbf{r}_e}{\partial \mathbf{u}_e} \mathbf{L}_e \quad (42)$$

where the derivative of  $\mathbf{r}_e$  with respect to  $\mathbf{u}_e$  is given by

$$\frac{\partial \mathbf{r}_e}{\partial \mathbf{u}_e} = \frac{\partial \mathbf{r}_e}{\partial \beta} \frac{\partial \beta}{\partial \mathbf{u}_{pe}} \frac{\partial \mathbf{u}_{pe}}{\partial \mathbf{u}_e} = \mathbf{z}_e \frac{\partial \beta}{\partial \mathbf{u}_{pe}} \mathbf{T}_e \quad (43)$$

with

$$\mathbf{z}_e^T = [\sin\beta \quad -\cos\beta \quad -\sin\beta \quad \cos\beta] \quad (44)$$

and

$$\frac{\partial \beta}{\partial \mathbf{u}_{pe}} = \frac{\mathbf{z}_e^T}{\ell_{pe}} \quad (45)$$

The geometric stiffness matrix of the tendon is then given by

$$\mathbf{K}_{Gp} = \sum_{e=1}^{n_p} \mathbf{L}_e^T \mathbf{K}_{Gpe} \mathbf{L}_e = \mathbf{A} \begin{pmatrix} \mathbf{K}_{Gpe} \end{pmatrix}_{e=1}^{n_p} \quad (46)$$

where

$$\mathbf{K}_{Gpe} = \left( \frac{F_p}{\ell_{pe}} \right) \mathbf{T}_e^T \mathbf{z}_e \mathbf{z}_e^T \mathbf{T}_e \quad (47)$$

corresponds to the geometric stiffness matrix of a tendon segment. According to the above expressions the geometric stiffness is a symmetric matrix with the same sparsity pattern than the stiffness matrix of the embedding beam.

Finally, the tangent stiffness matrix of the prestressing tendon is the sum of the material and geometric stiffness matrices:

$$\mathbf{K}_{Tp} = \mathbf{K}_{Ep} + \mathbf{K}_{Gp} \quad (48)$$

Due to the characteristics of its two components, this is a symmetric and dense matrix.

#### 4. Material models

Material nonlinearity is considered in the present model by nonlinear uniaxial stress-strain relations for the prestressing tendon, the concrete and the reinforcement. A large number of such stress-strain relations have been proposed, especially for the concrete component, and there is no agreement in the literature as to which equation leads to the best numerical behaviour, or even to the best fit of experimental data. Issues such as softening and confinement for the concrete and tendon stiffening for the reinforcement play important roles on the definition of these relations.

The FE formulation of the beam and tendon elements allows for different stress-strain relations to be considered, as long as the uniaxial constitutive equation and its first derivative are available. Only monotonic loading situations are considered, avoiding the use of more sophisticated plasticity or damage models.

##### 4.1. Concrete

Among the concrete models available, two have been adopted in the numerical assessments. The first one was used by Zupan and Saje [27]. It is composed of a single expression ranging from the ultimate compressive strain in the concrete  $\varepsilon_{cu}$  to  $\varepsilon_{ctr}$ , the value of strain corresponding to the resistance of the concrete in tension, and a straight line from this peak tensile stress to zero, attained at the maximum tensile strain  $\varepsilon_{ctu}$ :

$$\sigma_c = \begin{cases} f_c \frac{2 + \varepsilon_{c0} + \varepsilon_c}{\varepsilon_{c0} + \varepsilon_c^2} & \varepsilon_{cu} \leq \varepsilon_c \leq \varepsilon_{ctr} \\ f_{ctr} \frac{\varepsilon_c - \varepsilon_{ctu}}{\varepsilon_{ctr} - \varepsilon_{ctu}} & \varepsilon_{ctr} \leq \varepsilon_c \leq \varepsilon_{ctu} \end{cases} \quad (49)$$

This model is numerically convenient as a single smooth expression is used from the tension to the compression ranges, with a straight segment after peak tension stress. The four model input parameters are  $\varepsilon_{cu}$ ,  $\varepsilon_{c0}$ ,  $\varepsilon_{ctr}$ ,  $\varepsilon_{ctu}$  and  $f_c$ , which is concrete compressive resistance.

When concrete confinement by the transverse reinforcement must be taken into account, the stress-strain model from Scott and coworkers [28] for the compressive region was also considered. This relation involves a large set of initial parameters, namely: the concrete peak compressive stress  $f_c$ , the concrete ultimate strain  $\varepsilon_{cu}$ , the transverse reinforcement yield stress  $f_{yh}$ , the ratio of volume of hoop reinforcement to concrete  $Q_s$ , center-to-center hoop reinforcement spacing  $s_h$ , the confined concrete core width  $h$ , the elastic modulus of steel  $E_s$ .

The expressions for this uniaxial constitutive relation under compression are

$$\sigma_c = \begin{cases} -0.2Kf_c & \varepsilon_{cu} \leq \varepsilon_c \leq \varepsilon_{c,min} \\ -Kf_c(1 + Z(\varepsilon_c + \varepsilon_{c0})) & \varepsilon_{c,min} \leq \varepsilon_c \leq \varepsilon_{c0} \\ -Kf_c(1 - (1 + (\frac{\varepsilon_c}{\varepsilon_{c0}})^2)) & \varepsilon_{c0} \leq \varepsilon_c \leq 0 \end{cases} \quad (50)$$

In the previous equations, one has the definitions  $\varepsilon_{c0} = 0.002K$  and  $\varepsilon_{c,min} = \varepsilon_{c0} + \frac{0.8}{Z}$  where

$$K = 1 + Q_s \frac{f_{yh}}{f_c};$$

and

$$Z = \frac{0.5}{\frac{3 + 0.29f_c}{145f_c - 1000} + 0.75Q_s \sqrt{\frac{h}{s_h}} - 0.002K}$$

where  $f_c$  is in MPa units. In order to consider the influence of concrete under tension, and the tension stiffening effect, a constitutive model for concrete under tension after cracking was proposed by Hernández-Montes et al. [29], based on a previous exponential decay model developed by Stramandinoli and La Rovere [30]. According to this model, the stress-strain relationship is linear with elastic modulus  $E_c$  until the peak tensile stress for concrete  $f_{ct}$  is reached. After that, the tensile stress decays in a nonlinear fashion:

$$\sigma_c = \begin{cases} E_{ci} \varepsilon_c & 0 \leq \varepsilon_c \leq \varepsilon_{cr} \\ -\frac{E_s \rho \varepsilon_c}{2} + \sqrt{\left(\frac{E_s \rho \varepsilon_c}{2}\right)^2 + f_{ct}^2 (n\rho + 1)} & \varepsilon_{cr} \leq \varepsilon_c \leq \varepsilon_{ctu} \end{cases} \quad (51)$$

In the previous equations, the elastic concrete modulus  $E_{ci}$  may be taken as the CEB prescription (MPa)

$$E_{ci} = 2.15 \times 10^4 \sqrt[3]{\frac{f_c}{10}} \quad (52)$$

and the strain  $\varepsilon_{cr}$  is given as

$$\varepsilon_{cr} = \frac{f_{ct}}{E_{ci}} \quad (53)$$

Also, the symbols  $n = \frac{E_s}{E_{ci}}$  for the modular ratio and  $\rho = \frac{A_s}{A_c}$  for the reinforcement ratio are used, where  $A_s, A_c$  are the equivalent areas of reinforcement and concrete [30].

##### 4.2. Prestressing and reinforcing steel

The constitutive relation adopted for the prestressing steel is that from Menegotto and Pinto [31], given by the single expression valid only in tension

$$\sigma_p = \varepsilon_p E \left[ Q + (1-Q) \left( 1 + \left( \frac{E \varepsilon_p}{K \sigma_{py}} \right)^R \right)^{1/R} \right] \leq \sigma_{pu} \quad (54)$$

where  $E_p$  is the initial elastic modulus,  $\sigma_{py}$  is the conventional yield stress (corresponds to a yield strain equal 0.01), and  $K, Q$  and  $R$  are nondimensional coefficients which may be adjusted to improve fit to experimental data.

A bilinear model is adopted for the reinforcing steel, under either tension or compression:

$$\sigma_s = \begin{cases} -f_y - E_{sh}(\varepsilon_s + \varepsilon_{sy}) & -\varepsilon_{su} \leq \varepsilon_s \leq -\varepsilon_{sy} \\ E_s \varepsilon_s & -\varepsilon_{sy} \leq \varepsilon_s \leq \varepsilon_{sy} \\ f_y + E_{sh}(\varepsilon_s - \varepsilon_{sy}) & \varepsilon_{sy} \leq \varepsilon_s \leq \varepsilon_{su} \end{cases} \quad (55)$$

#### 5. Nonlinear analysis

The main aim of the nonlinear analysis of prestressed beams is to obtain their load-displacement curves, which allows to assess the deflections, load-carrying capacity, ductility and other important structural parameters. This curve is obtained solving the nonlinear equilibrium equations of the finite element model:

$$\mathbf{r}(\mathbf{u}, \lambda) = \mathbf{g}(\mathbf{u}) - \lambda \mathbf{q} = \mathbf{0} \quad (56)$$

where  $\mathbf{r}$  is the residual force vector,  $\mathbf{g}$  is the internal force vector,  $\mathbf{q}$  is the reference vector for the external loads and  $\lambda$  the load factor which scales the external loads. In the model presented in this work, both beam and tendon are considered as resisting elements, contributing to the internal force vector.

The nonlinear analysis of prestressed beams with unbonded tendons



requires two separate steps. The first step corresponds to the prestressing operation, which is the evaluation of the displacement field which results in tendon force  $F_p$  equal to the given equivalent prestressing force  $F_{pe}$ , assumed constant.

In practice, there are two ways to introduce prestressing on concrete beams. They will be briefly described here under the ideal assumption of zero prestress loss.

Pretensioning employs a device that applies and holds fixed an initial stress  $\sigma_{p0}$ , correspondent to a strain  $\varepsilon_{p0}$ , to the tendon. After, this initially stressed tendon is connected to the concrete beam (which may be cast after the tendon prestressing) at some discrete points (unbonded pretensioned beam) or continuously in contact with the concrete (bonded pretensioned beam). Upon release from the device, self-equilibrating forces develop in the beam-tendon system, which will give rise to a displacement field  $\mathbf{u}$  and reduce the initial strain (and force) on the tendon.

Post-tensioning, on the other hand, consists on applying an increasing force to both the tendon and the concrete element. Tension strains on the tendon and compressive strains on the concrete element develop gradually, with or without the influence of friction, until a specified force (or tendon elongation) is reached. At this point an anchoring system is attached to the prestressing end, in order to keep the beam under this self-equilibrating force system.

Regardless of the way the prestress was introduced, for the final tendon force  $F_{pe}$  corresponds an equilibrium state described by the beam and the linked tendon displacements. In most cases, however, the only information available is this final tendon force.

With the FE model used on this paper, the tendon material points are not followed, and there is no information on the differential displacements of the tendon and the concrete which would allow the evaluation of the strains in the case of post-tensioning. Nonetheless, it is enough to obtain the final equilibrium state, regardless of the prestressing scheme employed. For this reason, the simulation of the prestressing operation in the present work may be interpreted as the application of a pretensioning operation with initial strain  $\varepsilon_{p0}$  which is initially unknown. The consideration of this fixed initial strain allows the subsequent incremental strain calculations to be evaluated from Eq. (24), since after the release of the tendon in the pretensioning, or the anchoring in post-tensioning, the endpoints of the tendon are always at known positions.

Therefore, as a first step in the structural analysis, the initial strain resulting in a tendon force  $F_{pe} = A_p \sigma_{pe}$  and in equilibrium with the beam must be evaluated. Eq. (56) should be solved for  $\lambda = 0$  (no external loads) and an unknown  $\varepsilon_{p0}$ , resulting in the nonlinear system

$$\hat{\mathbf{r}} = \begin{bmatrix} \mathbf{g}(\mathbf{u}, \varepsilon_{p0}) \\ F_p(\mathbf{u}, \varepsilon_{p0}) - F_{pe} \end{bmatrix} = \begin{bmatrix} \mathbf{0} \\ 0 \end{bmatrix} \quad (57)$$

This nonlinear system with  $n + 1$  variables and  $n + 1$  equations can be solved using the Newton-Raphson method and may be interpreted as a variant of the usual path-following methods in which the step is stress-controlled. The linearization of this system results in

$$\mathbf{g} + \frac{\partial \mathbf{g}}{\partial \mathbf{u}} \delta \mathbf{u} + \frac{\partial \mathbf{g}}{\partial \varepsilon_{p0}} \delta \varepsilon_{p0} = 0$$

$$F_p - F_{pe} + \frac{\partial F_p}{\partial \mathbf{u}} \delta \mathbf{u} + \frac{\partial F_p}{\partial \varepsilon_{p0}} \delta \varepsilon_{p0} = 0 \quad (58)$$

where  $i$  is the iteration number and  $\delta \mathbf{u}$  and  $\delta \varepsilon_{p0}$  are the iterative corrections. The internal force of the structure is given by

$$\mathbf{g} = \mathbf{g}_b + \mathbf{g}_p = \mathbf{g}_b + F_p \mathbf{w} \quad (59)$$

Since the internal force vector of the beam elements ( $\mathbf{g}_b$ ) does not depend on the initial prestressing strain  $\varepsilon_{p0}$ :

$$\frac{\partial \mathbf{g}}{\partial \varepsilon_{p0}} = \frac{\partial F_p}{\partial \varepsilon_{p0}} \mathbf{w} = A_p \frac{\partial \sigma_p}{\partial \varepsilon_p} \frac{\partial \varepsilon_p}{\partial \varepsilon_{p0}} \mathbf{w} = A_p E_{pt} \mathbf{w} \quad (60)$$

In addition, using Eq. (39):

$$\frac{\partial F_p}{\partial \mathbf{u}} = A_p \frac{\partial \sigma_p}{\partial \varepsilon_p} \frac{\partial \varepsilon_p}{\partial \mathbf{u}} = \frac{A_p E_{pt}}{L_p} \mathbf{w}^T \quad (61)$$

Therefore, Eq. (58) can be written as

$$\begin{cases} \mathbf{K}_T \delta \mathbf{u} + \delta \varepsilon_{p0} A_p E_{pt} \mathbf{w} = -\mathbf{g} \\ \frac{A_p E_{pt}}{L_p} \mathbf{w}^T \delta \mathbf{u} + A_p E_{pt} \delta \varepsilon_{p0} = F_{pe} - F_p \end{cases} \quad (62)$$

In order to efficiently solve this system, the displacement increment is written as

$$\delta \mathbf{u} = \delta \mathbf{u}_1 + \delta \varepsilon_{p0} \delta \mathbf{u}_2 \quad (63)$$

where

$$\begin{cases} \mathbf{K}_T \delta \mathbf{u}_1 = -\mathbf{g} \\ \mathbf{K}_T \delta \mathbf{u}_2 = -A_p E_{pt} \mathbf{w} \end{cases} \quad (64)$$

The substitution of Eq. (63) in the second line of Equation (62) yields the strain increment:

$$\delta \varepsilon_{p0} = \frac{(F_{pe} - F_p) L_p - A_p E_{pt} \mathbf{w}^T \delta \mathbf{u}_1}{A_p E_{pt} (\mathbf{w}^T \delta \mathbf{u}_2 + L_p)} \quad (65)$$

Thus, the displacements and the initial prestressing strain are updated in each iteration as

$$\begin{aligned} \mathbf{u}_{i+1} &= \mathbf{u}_i + \delta \mathbf{u} \\ \varepsilon_{p0i+1} &= \varepsilon_{p0i} + \delta \varepsilon_{p0} \end{aligned} \quad (66)$$

where  $\delta \mathbf{u}$  is computed using Eq. (63). This iterative procedure can be stopped when

$$\frac{\|\hat{\mathbf{r}}\|}{F_{pe}} \leq \text{TOL} \quad (67)$$

where TOL is the prescribed tolerance for convergence. This iterative procedure is very robust and converges in few steps, and may be initialized with  $\mathbf{u} = \mathbf{0}$  and  $\varepsilon_{p0} = 0$ .

The second step is the analysis of the beam under external loading considering the initial prestressing strain ( $\varepsilon_{p0}$ ) evaluated in the first step. To this end, Eq. (56) may be solved using the Newton-Raphson method for increasing  $\lambda$ . However, as these beams tend to fail after reaching limit points, this simple load control approach cannot trace the complete load-displacement curve. Thus, in order to capture effectively the behavior of these structures, a displacement control strategy with Newton-Raphson iterations [32] is adopted for the load application stages in this work.

## 6. Applications

This section presents the validation of the proposed formulation for nonlinear analysis of post-tensioned beams with unbonded tendons based on the comparison of finite element responses with experimental results.

### 6.1. Unbonded prestressed concrete beam with curved tendon

A set of unbonded prestressed concrete beams was tested by Hussien et al. [33]. The specimen called B7 is a simply supported beam under four-point bending load, with rectangular cross section and tendon profile as indicated in Fig. 4. Upper and lower reinforcement with 1.57 cm<sup>2</sup> each are positioned 4 cm distant from the top and bottom faces of the beam. The prestressing tendon is anchored at the centroid of end cross-sections and its lowest segment lies at 4.3 cm from the bottom of the beam. The tendon has area of 0.99 cm<sup>2</sup> and the prestressing, after initial losses, is assumed as 1000 MPa.

The only concrete parameter available in [33] is the compressive resistance of 43 MPa. Following the Eurocode guidelines, the peak compressive strain was estimated as  $2.246 \times 10^{-3}$  and the ultimate

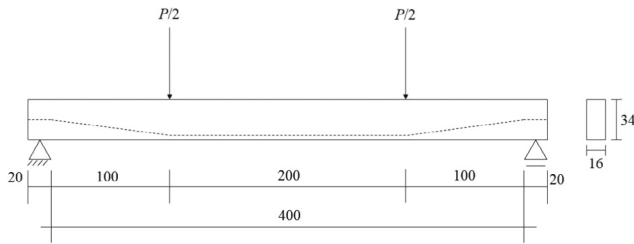


Fig. 4. Prestressed beam from [33] (units in cm).

compressive strain was taken as  $3.1 \times 10^{-3}$ . The peak and ultimate tensile strains were estimated as  $1 \times 10^{-5}$  and  $4 \times 10^{-4}$ , respectively for use with the Zupan and Saje [27] concrete model. The parameters adopted for the steel reinforcement were: yield stress of 470 MPa, elastic modulus 210 GPa, hardening modulus 1.2 GPa and ultimate strain 0.12. The prestressing tendon has a yield stress of 1674 MPa, ultimate stress of 1860 MPa, elastic modulus 195 GPa, ultimate strain of 0.06 and  $K, Q$  and  $R$  taken as 1.04, 0.012 and 8.127, respectively.

Three meshes with 6, 10 and 18 beam elements were employed in the numerical analysis, with a uniform discretization of 4, 8 and 16 elements between the supports, respectively. Element integration was performed using 2 Gauss points and cross sectional integration was carried out using 50 layers. The nonlinear analysis was performed incrementing the vertical displacement ( $v$ ) of the central node in 20 increments of 5 mm and a tolerance for convergence of  $10^{-5}$ . The load-displacement curves of the central node are shown in Fig. 5. It can be noted that the finite element results are in very good agreement with the experimental results, even for the coarser (6 element) mesh. The results with finer meshes are practically identical.

This example was chosen to assess the convergence properties of the proposed FE scheme. Table 1 presents the iterative results of the first analysis step for the 18-element mesh, corresponding to the prestress application and prior to the external load increments. It can be noted that the procedure proposed in this work presents a fast convergence rate due to the adoption of the Newton-Raphson method with the consistent linearization of the residual vector.

The iterations corresponding of the last displacement increment ( $v = 100$  mm) are presented in Table 2. These results show that the formulation proposed in this work, where the stiffness matrix of the prestressing tendon is obtained by the consistent linearization of the internal forces, ensures the optimal quadratic convergence of the Newton-Raphson iterations.

The same example, with the 6-element mesh under a displacement control step of 10 mm and a total of 10 steps is considered next. Fig. 6

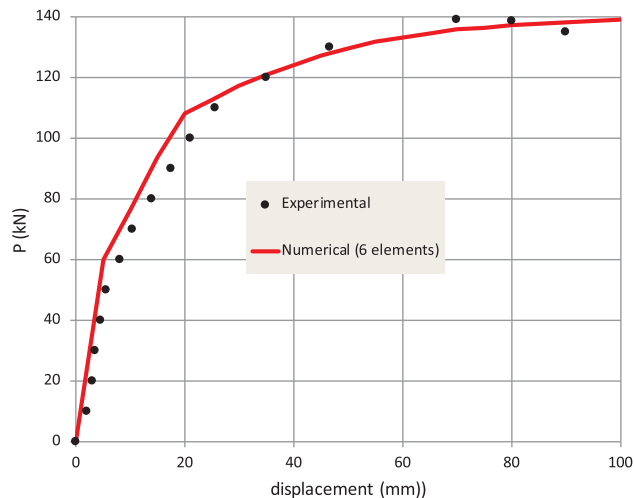


Fig. 5. Load-displacement curve of Example 1.

Table 1  
Convergence of prestress application.

Iter	$\epsilon_{p0}$	$\sigma_p$ (Pa)	$\ \mathbf{r}\ /F_{pe}$
1	$0.000000 \times 10^0$	$0.000000 \times 10^0$	$1.000000 \times 10^0$
2	$5.219815 \times 10^{-3}$	$9.987055 \times 10^8$	$1.322045 \times 10^{-1}$
3	$5.232335 \times 10^{-3}$	$1.000003 \times 10^9$	$4.400811 \times 10^{-2}$
4	$5.233903 \times 10^{-3}$	$1.000001 \times 10^9$	$7.977834 \times 10^{-3}$
5	$5.234049 \times 10^{-3}$	$1.000000 \times 10^9$	$2.544561 \times 10^{-6}$

Table 2  
Convergence of the last displacement increment.

Iter	$\lambda$	$\ \mathbf{r}\ /\ \mathbf{q}\ $
1	138.975438	$2.676338 \times 10^1$
2	138.943002	$1.849663 \times 10^{-1}$
3	138.942995	$6.738832 \times 10^{-5}$
4	138.942996	$4.254647 \times 10^{-8}$

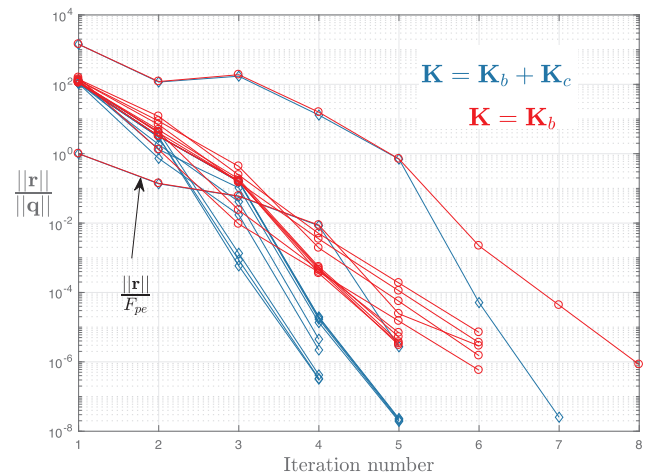


Fig. 6. Convergence analysis.

displays the evolution of the error associated with each analysis step, with and without the consideration of the tendon contribution to the tangent stiffness matrix. Also shown is the convergence analysis of the prestressing step for which the error parameter is given by  $\|\mathbf{r}\|/F_{pe}$ . It is clear from the graphics that the presence of the tendon stiffness  $K_c$  improves the convergence rates restoring the optimal rates of the Newton-Raphson scheme. It is worth noting that if the analysis is extended until a target final displacement of 200 mm in 20 steps, without the tendon stiffness, the 6, 10 and 18-element meshes stop at steps 13, 11 and 10 respectively. The full consistent matrix, however, is able to trace the path up to the final step.

### 6.2. Unbonded prestressed concrete beams with straight tendon

Tao and Du [34] carried out a series of tests of 22 simply supported unbonded prestressed concrete beams. The span for all the specimens was 4.20 m and the beams are subject to a four-point load scheme, as depicted in Fig. 7.

Nine specimens for the group A of beams were analyzed by the present numerical procedure. These examples include beams with different reinforcement ratios and prestressing forces, and Table 3 displays details for each specimen (stresses in MPa, areas in  $\text{cm}^2$  and strains in  $\text{mm/m}$ ). The beam cross sections were 16 cm wide and 28 cm deep, with the position from the top fiber of the reinforcement bars and the prestressing tendon 25 cm and 22 cm respectively. The prestressing tendon, which is straight for every specimen, has a yield stress of

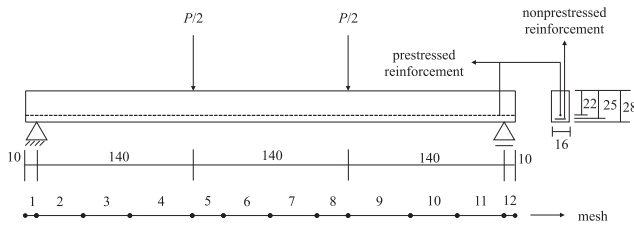


Fig. 7. Prestressed beams of [34] (units in cm).

Table 3  
Data for postensioned beams by Tao and Du [34].

Beam	$f_c$	$f_y$	$A_s$	$A_p$	$\sigma_{pe}$	$\epsilon_{c0}$	$\epsilon_{cu}$
A1	30.6	267	1.57	0.588	960	2.021	4.0
A2	30.6	430	1.57	0.980	904	2.021	6.0
A3	30.6	430	2.36	1.568	820	2.021	6.0
A4	30.6	430	1.57	0.588	869	2.021	6.0
A5	30.6	430	3.08	0.784	810	2.021	4.5
A6	30.6	400	4.62	1.568	854	2.021	4.0
A7	30.6	400	3.08	0.392	885	2.021	6.0
A8	33.1	400	4.62	0.588	894	2.071	4.0
A9	33.1	395	8.04	1.568	920	2.071	4.0

1465 MPa, ultimate stress of 1790 MPa, elastic modulus 205 GPa, ultimate strain of 0.06 and coefficients  $K, Q$  and  $R$  taken as 1.04, 0.02472 and 4.6019, respectively. Additionally, the concrete strain  $\epsilon_{cr}$  is taken as  $1.0^{-5}$ , the  $E_{sh}$  modulus of reinforcement is 1.2 GPa and its ultimate strain  $\epsilon_{su}$  is 0.16. The model described by Eqs. (49) is employed for the concrete. Twelve frame elements were employed in the numerical simulation. Cross-section integration was carried-out using 50 layers. Tolerance for convergence in nonlinear analysis was taken as  $10^{-4}$ .

For the beams, The FE and experimental load-displacement curves at the mid-span are presented in Figs. 8 and 9, while the increase in tendon stress are depicted in Figs. 10 and 11. It can be noted that the proposed model was able to obtain the complete load-displacement curves of all beams, showing its robustness. In addition, the agreement between the finite element and experimental results vary from good to excellent, for both load-displacements and evolution of tendon stresses.

It is worth noting the three distinct phases of the load-displacement curves for the beams in this example. Initially an elastic behaviour is evident, with very similar stiffness for all beams. After cracking the beam stiffness is reduced and after yielding the ultimate load is reached. For specimens A3, A6 and A9, which have the highest values of prestressing tendon areas, the gain in ultimate resistance comes at a price of much less ductile behaviour.

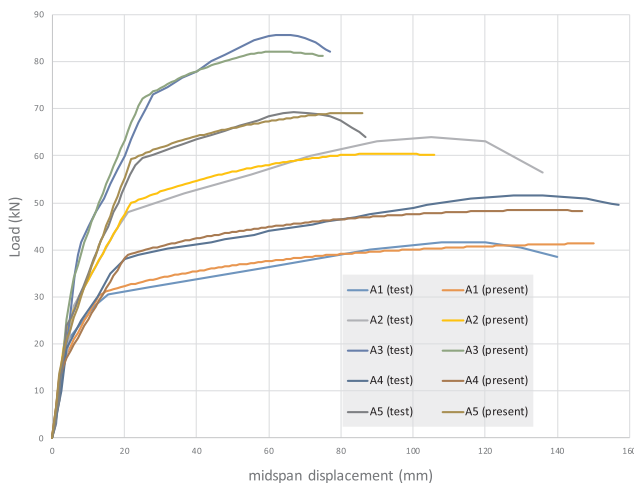


Fig. 8. Load-displacement curves (beams A1 to A5).

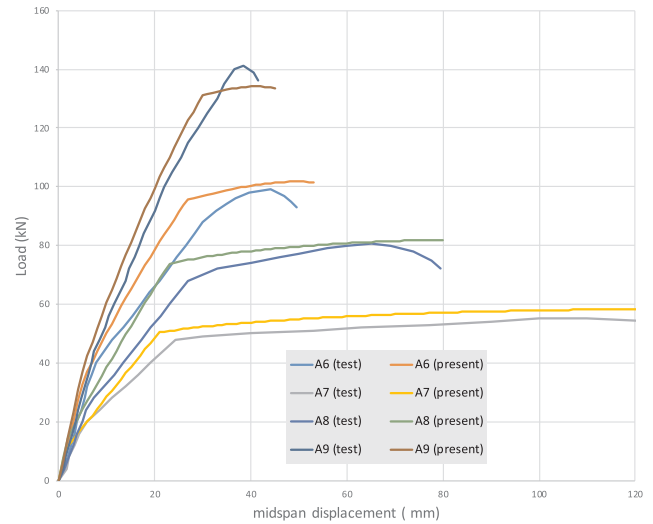


Fig. 9. Load-displacement curves (beams A6 to A9).

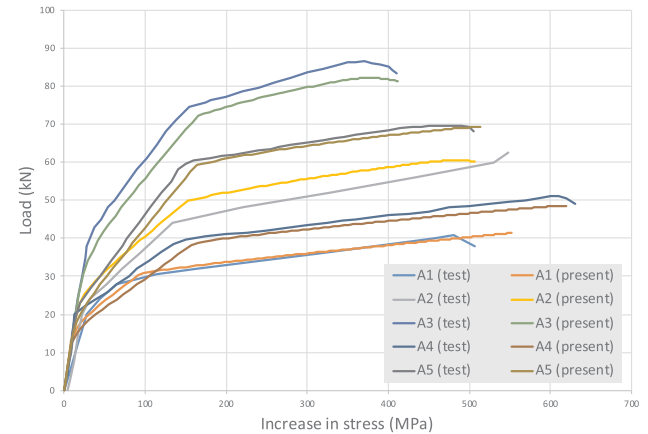


Fig. 10. Tendon stress increase (beams A1 to A5).

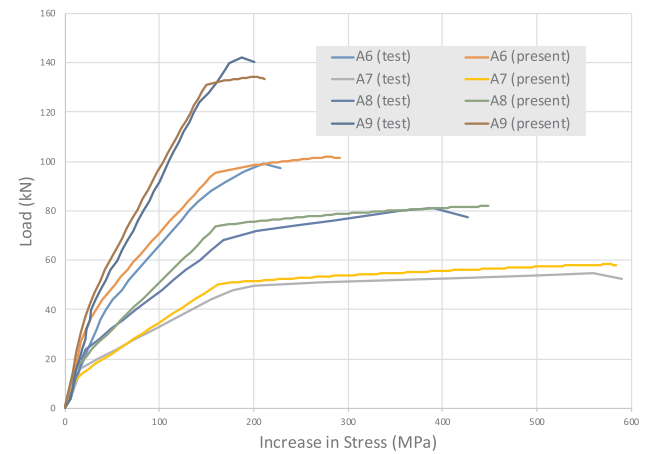


Fig. 11. Tendon stress increase (beams A6 to A9).

### 6.3. Continuous unbonded prestressed beams

In this section, a series of five two-span continuous unbonded prestressed concrete beams with curved tendons are analyzed with the proposed methodology. These beams have been studied by Lou, Lopes and Lopes [13] from which the results presented were obtained. The geometry of the continuous beam is depicted in Fig. 12, where the positions of the tendon and reinforcements are shown.



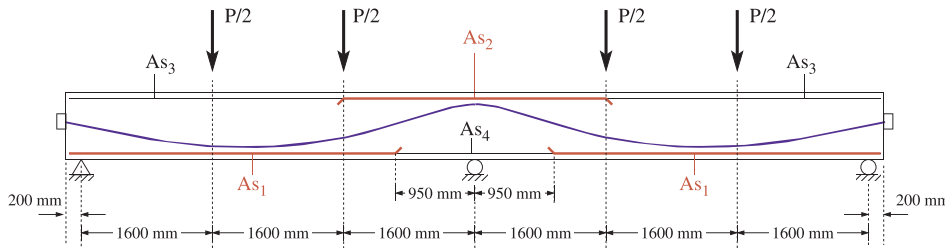


Fig. 12. Two-span prestressed beam geometry.

Table 4  
Reinforcements and initial pretension.

Beam	As <sub>1</sub>	As <sub>2</sub>	As <sub>3</sub>	As <sub>4</sub>	f <sub>pe</sub>
YLA1	4Ø12	2Ø12	2Ø12	2Ø12	1083
YLA2	4Ø12	2Ø12	2Ø12	2Ø12	1196
YLB2	3Ø16	2Ø18	2Ø12	3Ø16	1193
YLC1	3Ø18	3Ø18	2Ø12	3Ø18	1169
YLC2	3Ø18	3Ø18	2Ø12	3Ø18	1205

The beam sections are rectangular with 150 mm width and 300 mm height and each span is 4800 mm long. Reinforcement bars lie at 35 mm from the top/bottom of the concrete section. The layout of the tendons was the same for all beams, the position of the tendon being defined by piecewise quadratic equations [13]. Seven-wire 15 mm strands are used for the prestressing tendons, with ultimate strength, yield strength and elastic modulus of 1941 MPa, 1680 MPa and 197 GPa, respectively. The reinforcement consisted of 12, 16 or 18 mm diameter bars with yield strengths of 361, 384 and 364 MPa, respectively. The shear reinforcement consisted of 10 mm stirrups with spacing of 150 mm in the outer shear spans and of 200 mm in the flexural spans for all beams, while the shear reinforcement in the inner shear spans consisted of 10 mm stirrups with spacing of 150 mm for Beams YLA1 and YLA2, 100 mm for Beam YLB2 and 80 mm for Beams YLC1 and YLC2. The reinforcements A<sub>s</sub> and effective prestress values f<sub>pe</sub> for the beams are shown in Table 4. The areas of the Ø12, Ø16 and Ø18 reinforcement bars were considered as 113, 201 and 254 mm<sup>2</sup> respectively. For the rebars, the elastic modulus is taken as 200 GPa.

The material model employed for the concrete was the one by Scott and coworkers [28] for the compression behaviour and, for the behavior under tension, the model of Hernández-Montes et al. [29]. Table 5 displays the necessary parameters for the employment of these constitutive equations (dimensions in mm and stresses in MPa). Moreover, the yield stress of the transverse bars f<sub>yh</sub> is taken as 360 MPa. For all the beams the ultimate concrete strain in tension ε<sub>ctu</sub> was taken as 0.001. The stirrup spacing s<sub>h</sub> takes the values of 80, 100, 150 or 200 mm as explained above.

In order to assess the results of the FE analysis, once again load-displacement curves are employed. Figs. 13–17 show the load-displacement relations for the five beams analyzed and they match closely the numerical results from [13]. A very good agreement for the tendon force evolution with the applied load was also obtained.

Table 5  
Parameters for the concrete model of the continuous beams.

Beam	f <sub>c</sub>	ε <sub>cu</sub>	Q <sub>s</sub>	h	f <sub>ct</sub>	ρ
YLA1	34.9	0.01764	0.01263	262	1.5	0.010
YLA2	36.7	0.01764	0.01263	262	0.8	0.005
YLB2	33.0	0.01727	0.01229	266	1.0	0.013
YLC1	37.1	0.01708	0.01211	268	0.8	0.017
YLC2	33.2	0.01708	0.01211	268	0.6	0.017

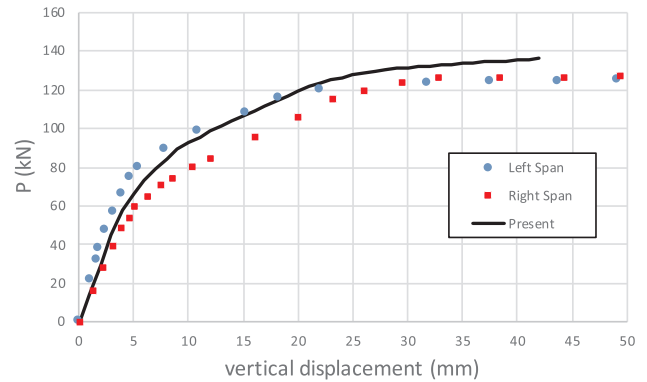


Fig. 13. Beam YLA1 load-displacement curve.

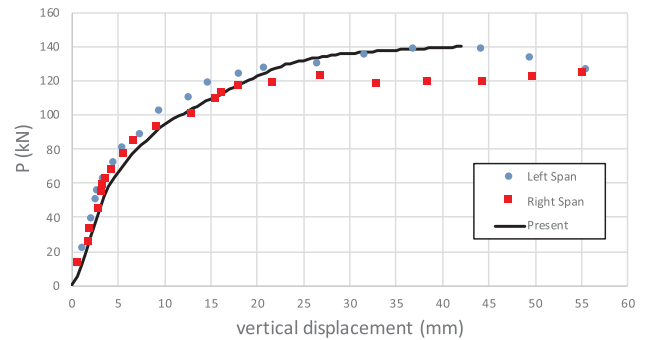


Fig. 14. Beam YLA2 load-displacement curve.

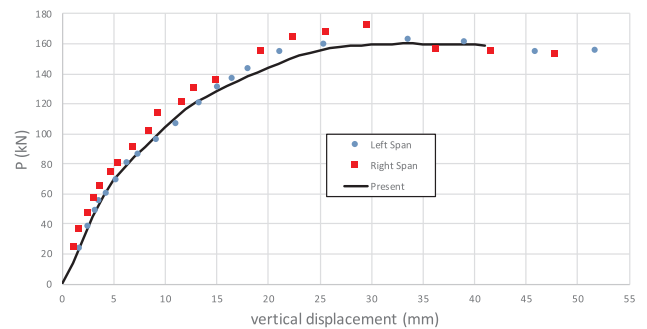


Fig. 15. Beam YLB2 load-displacement curve.

With the aim to identify precisely the performance of the specimens during the loading stage, two cross sections are analyzed in terms of steel and concrete strains and beam generalized strain (curvature). These are the sections over the support and a critical section of the flexural span. Fig. 18 display the evolution of the curvature of the two sections analyzed. As expected the section over the central support starts to gradually reduce its stiffness while the span critical section still exhibits an almost linear behaviour. Only when the load-curvature reaches its limit value for the cross section over the central support the

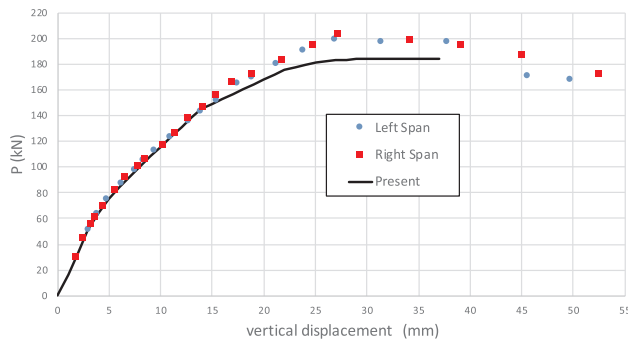


Fig. 16. Beam YLC1 load-displacement curve.

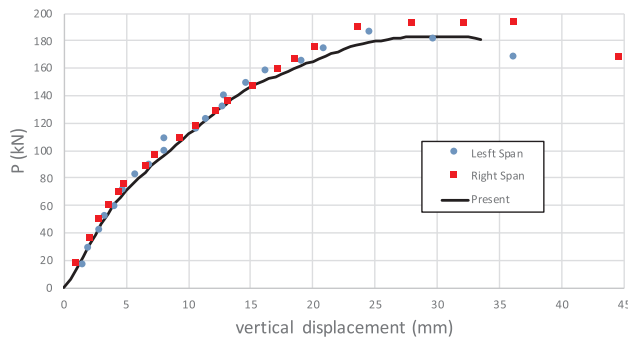


Fig. 17. Beam YLC2 load-displacement curve.

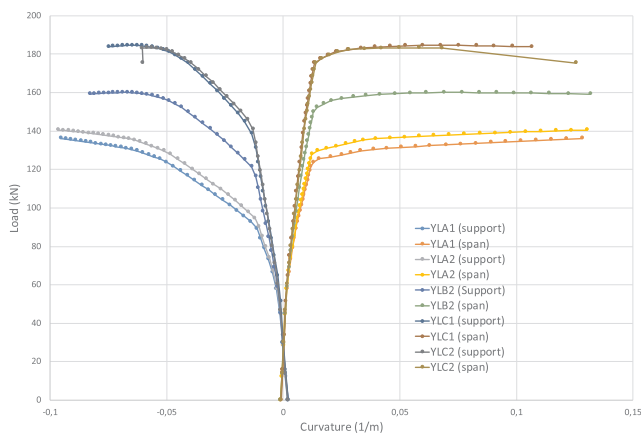


Fig. 18. Curvatures of central support and critical span position.

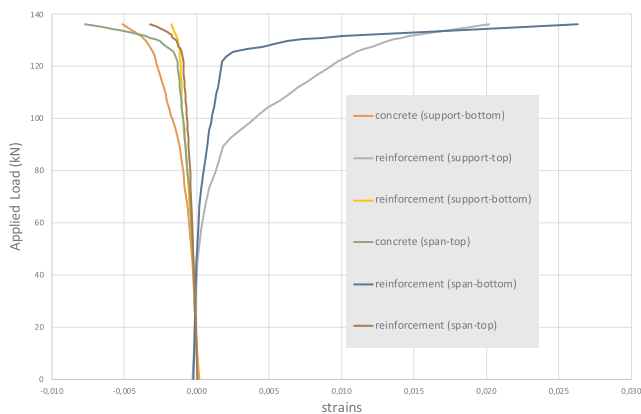


Fig. 19. Strains of concrete and rebars (central support and critical span position).

stiffness of the critical span section decreases abruptly. At the ultimate stages it becomes clear the formation of plastic hinges at these sections, with the span cross section displaying a more ductile behaviour.

The five beams have similar behaviour with respect to the evolution of strains until the ultimate load is reached. Initially, after application of prestress, the strains remain in the elastic range, and apparently there is no cracking. For relatively low levels of the applied force the concrete reaches its ultimate tension level almost simultaneously at the top of the central support and the bottom of the span critical section. After that there is the yielding of the reinforcement at the top of the central support, followed by yielding of the reinforcements at the bottom and the top of the critical section.

In order to investigate the evolution of strains at these cross sections, Fig. 19 has been produced, with respect to beam YLA1. It depicts the concrete strains at the bottom of the support section and the top of the span critical section, as well as the strains for the four reinforcements at the top and bottom of these two sections. It is possible to see the yielding of the reinforcements on the top of the support and the bottom of the critical span sections occur at load levels around 90 and 130 kN respectively. It is interesting to observe the ductile behaviour of the concrete at the top of the critical span section, where strains up to 0.007 arise. For this reason the concrete model that considers confinement must be used in this example.

### 7. Conclusions

This work presented a novel finite element model for the material and geometric nonlinear analysis of prestressed concrete beams with unbonded internal tendons, under short term loading.

In this model, the RC beam is discretized using nonlinear Euler-Bernoulli frame elements based on the Total Lagrangian approach, while the slipping tendon is modeled by a single cable element embedded in a specific subset of frame elements. The formulation of the tendon element is based on the engineering strain for large displacements, allowing the consideration of the variation of the tendon force and geometry along the analysis. The contribution of frame and tendon elements to the global internal force vector and stiffness matrix is evaluated in a consistent way, leading to a more robust and stable nonlinear solution. It was shown that if the nonlinear terms of the tendon stiffness matrix are not complete the convergence is slowed and may even not be reached. A novel stress control strategy was developed to simulate the prestressing step of the analysis. It is based on the imposition of equilibrium of the final tendon force with the internal beam forces, and by consideration of an initial reference strain, does not need to enforce compatibility.

The proposed formulation was tested against a series of experimental results and displayed very good agreement in terms of load-displacement curves, as well as tendon force evolution and other structural responses, along the complete loading history up to collapse. Therefore, the newly proposed FE model provides an important contribution for the simulation of prestressed beams with unbonded internal tendons.

### Acknowledgements

The authors wish to thank CNPq (Conselho Nacional de Desenvolvimento Científico e Tecnológico) (Grant Nos. 307643/2016-6 and 307616/2017-7) and FUNCAP (Fundação Cearense de Amparo à Pesquisa) for the support to this work.

### References

- [1] Aalami BO. Post-tensioned buildings design and construction, PT-Structures; 2014.
- [2] Lin TY, Burns NH. Design of prestressed concrete structures. Wiley; 1981.
- [3] Aalami B. Load balancing-a comprehensive solution to post-tensioning. ACI Struct J 1990;87(6):662–70.

- [4] Aalami B. Structural modeling of posttensioned members. *J Struct Eng New York, N.Y.* 2000;126(2):157–62. [http://dx.doi.org/10.1061/\(ASCE\)0733-9445\(2000\)126:2\(157\)](http://dx.doi.org/10.1061/(ASCE)0733-9445(2000)126:2(157)).
- [5] Barbieri RA, Gastal FPSL, Campos Filho A. Numerical model for the analysis of unbonded prestressed members. *J Struct Eng* 2006;132(1):34–42. [http://dx.doi.org/10.1061/\(ASCE\)0733-9445\(2006\)132:1\(34\)](http://dx.doi.org/10.1061/(ASCE)0733-9445(2006)132:1(34)).
- [6] Dall'Asta A, Zona A. Finite element model for externally prestressed composite beams with deformable connection. *J Struct Eng* 2005;131(5):706–14. [http://dx.doi.org/10.1061/\(ASCE\)0733-9445\(2005\)131:5\(706\)](http://dx.doi.org/10.1061/(ASCE)0733-9445(2005)131:5(706)).
- [7] Zona A, Ragni L, Dall'Asta A. Finite element formulation for geometric and material nonlinear analysis of beams prestressed with external slipping tendons. *Finite Elem Anal Des* 2008;44(15):910–9. <http://dx.doi.org/10.1016/j.finel.2008.06.005>.
- [8] Dall'Asta A, Ragni L, Zona A. Analytical model for geometric and material nonlinear analysis of externally prestressed beams. *J Eng Mech* 2007;133(1):117–21. [http://dx.doi.org/10.1061/\(ASCE\)0733-9399\(2007\)133:1\(117\)](http://dx.doi.org/10.1061/(ASCE)0733-9399(2007)133:1(117)).
- [9] Dall'asta A, Ragni L, Zona A. Simplified method for failure analysis of concrete beams prestressed with external tendons. *J Struct Eng* 2007;133(1):121–31. [http://dx.doi.org/10.1061/\(ASCE\)0733-9445\(2007\)133:1\(121\)](http://dx.doi.org/10.1061/(ASCE)0733-9445(2007)133:1(121)).
- [10] Zona A, Ragni L, Dall'Asta A. Simplified method for the analysis of externally prestressed steel-concrete composite beams. *J Constr Steel Res* 2009;65(2):308–13. <http://dx.doi.org/10.1016/j.jcsr.2008.07.015>.
- [11] Lou T, Xiang Y. Finite element modeling of concrete beams prestressed with external tendons. *Eng Struct* 2006;28(14):1919–26. <http://dx.doi.org/10.1016/j.engstruct.2006.03.020>.
- [12] Lou T, Xiang Y. Numerical analysis of second-order effects of externally prestressed concrete beams. *Struct Eng Mech* 2010;35(5):631–43.
- [13] Lou T, Lopes S, Lopes A. Nonlinear and time-dependent analysis of continuous unbonded prestressed concrete beams. *Comp Struct* 2013;119:166–76. <http://dx.doi.org/10.1016/j.compstruc.2012.12.014>.
- [14] Lou T, Lopes S, Lopes A. A finite element model to simulate long-term behavior of prestressed concrete girders. *Finite Elem Anal Des* 2014;81:48–56. <http://dx.doi.org/10.1016/j.finel.2013.11.007>.
- [15] Lou T, Lopes S, Lopes A. A comparative study of continuous beams prestressed with bonded frp and steel tendons. *Compos Struct* 2015;124:100–10. <http://dx.doi.org/10.1016/j.compstruct.2015.01.009>.
- [16] Lou T, Lopes S, Lopes A. Response of continuous concrete beams internally prestressed with unbonded frp and steel tendons. *Compos Struct* 2016;154:92–105. <http://dx.doi.org/10.1016/j.compstruct.2016.07.028>.
- [17] Lou T, Lopes S, Lopes A. Fe analysis of short- and long-term behavior of simply supported slender prestressed concrete columns under eccentric end axial loads causing uniaxial bending. *Eng Struct* 2015;85:52–62. <http://dx.doi.org/10.1016/j.engstruct.2014.12.023>.
- [18] Lou T, Lopes S, Lopes A. Numerical modeling of externally prestressed steel-concrete composite beams. *J Constr Steel Res* 2016;121:229–36. <http://dx.doi.org/10.1016/j.jcsr.2016.02.008>.
- [19] Vu N, Castel A, François R. Response of post-tensioned concrete beams with unbonded tendons including serviceability and ultimate state. *Eng Struct* 2010;32(2):556–69. <http://dx.doi.org/10.1016/j.engstruct.2009.11.001>.
- [20] Kim KS, Lee DH. Nonlinear analysis method for continuous post-tensioned concrete members with unbonded tendons. *Eng Struct* 2012;40:487–500. <http://dx.doi.org/10.1016/j.engstruct.2012.03.021>.
- [21] Crisfield MA. *Non-linear finite element analysis of solids and structures vol. 1.* John Wiley and Sons; 1991.
- [22] Sousa Jr. JBM, Caldas RB. Numerical analysis of composite steel-concrete columns of arbitrary cross section. *J Struct Eng* 2005;131(11):1721–30. [http://dx.doi.org/10.1061/\(ASCE\)0733-9445\(2005\)131:11\(1721\)](http://dx.doi.org/10.1061/(ASCE)0733-9445(2005)131:11(1721)).
- [23] Sousa Jr. JBM, Muniz CFDG. Analytical integration of cross section properties for numerical analysis of reinforced concrete, steel and composite frames. *Eng Struct* 2007;29(4):618–25. <http://dx.doi.org/10.1016/j.engstruct.2006.06.002>.
- [24] Parente Jr E, Nogueira GV, Meireles Neto M, Moreira LS. Material and geometric nonlinear analysis of reinforced concrete frames. *Revista IBRACON de Estruturas e Materiais* 2014;7:879–904. <http://dx.doi.org/10.1590/S1983-41952014000500009>.
- [25] Naaman AE, Alkhairi FM. Stress at ultimate on unbonded post-tensioned tendons: Part 1 – evaluation of the state of the art. *ACI Struct J* 1991;88(5):641–51.
- [26] Naaman AE, Alkhairi FM. Stress at ultimate on unbonded post-tensioned tendons: Part 2 – proposed methodology. *ACI Struct J* 1991;88(6):683–92.
- [27] Zupan D, Saje M. Analytical integration of stress field and tangent material moduli over concrete cross-sections. *Comput Struct* 2005;83(28-30):2368–80. <http://dx.doi.org/10.1016/j.compstruc.2005.03.030>.
- [28] Scott RPB, Priestley MJN. Stress-strain behavior of concrete confined by overlapping hoops at low and high strain rates. *ACI J* 79(1). <http://dx.doi.org/10.14359/10875>.
- [29] Hernández-Montes E, Cesetti A, Gil-Martín LM. Discussion of an efficient tension-stiffening model for nonlinear analysis of reinforced concrete members, by renata s.b. stramandinoli, henriette l. la rovere. *Eng Struct* 2013;48:763–4. <http://dx.doi.org/10.1016/j.engstruct.2012.09.032>.
- [30] Stramandinoli RS, Rovere HLL. Fe model for nonlinear analysis of reinforced concrete beams considering shear deformation. *Eng Struct* 2012;35:244–53. <http://dx.doi.org/10.1016/j.engstruct.2011.11.019>.
- [31] Menegotto M, Pinto PE. Method of analysis for cyclically loaded reinforced concrete plane frames, including changes in geometry and non-elastic behavior of elements under combined normal force and bending. In: Preliminary report for symposium on resistance and ultimate deformability of structures acted on well-defined repeated loads, vol. 13 of IABSE, 1973. p. 15–22.
- [32] Batoz J-L, Dhatt G. Incremental displacement algorithms for nonlinear problems. *Int J Numer Meth Eng* 1979;14(8):1262–7. <http://dx.doi.org/10.1002/nme.1620140811>.
- [33] Hussien O, Elafandy T, Abdelrahman A, Baky SA, Nasr E. Behavior of bonded and unbonded prestressed normal and high strength concrete beams. *HBRC J* 2012;8(3):239–51. <http://dx.doi.org/10.1016/j.hbrj.2012.10.008>.
- [34] Tao X, Du G. Ultimate stress of unbonded tendons in partially prestressed concrete beams. *PCI J* 1985;30(6):72–91.